

Banner appropriate to article type will appear here in typeset article

# The merger of co-rotating vortices in dusty flows

Shuai Shuai<sup>1</sup> and Anubhab Roy<sup>2</sup> and M. Housseem Kasbaoui<sup>1</sup>†

<sup>1</sup>School for Engineering of Matter, Transport and Energy, Arizona State University, Tempe, AZ 85281, USA.

<sup>2</sup>Department of Applied Mechanics, Indian Institute of Technology Madras, Chennai, 600036, India.

(Received xx; revised xx; accepted xx)

We investigate the effect of particle inertia on the merger of co-rotating dusty vortex pairs at semi-dilute concentrations. Using Eulerian-Lagrangian simulations, we show substantial departure from the vortex dynamics previously established in particle-free flows. Most strikingly, we find that dispersed particles with moderate inertia cause the vortex pair to push apart to a separation nearly twice as large as the initial separation. We find that antisymmetric vorticity generated by particles flung out of the rotational cores causes the vortex pair repulsion. Eventually, the two dusty vortices merge into a single vortex with most particles accumulating outside the core similar to the dusty Lamb-Oseen vortex described in Shuai & Kasbaoui (*J. Fluid Mech.*, vol 936, 2022, A8). For weakly inertial particles, we find that the merger dynamics follow the same mechanics as those of a single-phase flow, albeit with a density that must be adjusted to match the mixture density. Lastly, highly inertial particles tend to fragment the vortex cores leading to murky merger dynamics.

**Key words:** keyword 1, keyword 2, keyword 3

## 1. Introduction

The majority of prior work on vortex merger concerned single-phase flows (Roberts & Christiansen 1972; Rossow 1977; Overman & Zabusky 1982), where it was shown that the merger of two co-rotating vortices with equal strength is initiated only once the ratio of vortex core size  $a$  to pair separation  $b$  reaches a critical value. If the ratio  $a/b$  is below  $(a/b)_{\text{crit}}$ , the two vortices rotate around one another, while their separation remains mostly constant and their sizes grow due to viscous diffusion. Melander *et al.* (1988) defined this stage as viscous metastable stage with a lifetime that depends on the dissipation time scale. As the vortices expand, the ratio  $a/b$  eventually reaches the critical threshold  $(a/b)_{\text{crit}}$  and the convective stage follows, in which the vortices move toward each other rapidly. Griffiths & Hopfinger (1987) found the the critical threshold to be  $(a/b)_{\text{crit}} = 0.29 - 0.32$  in water tank experiments. Later, Cerretelli & Williamson (2003) also found  $(a/b)_{\text{crit}} \approx 0.29$ . By analyzing the vorticity field, Cerretelli & Williamson (2003) determined that the merger is initiated once the two vortices are sufficiently close to generate antisymmetric vorticity, which occurs

† Email address for correspondence: houssem.kasbaoui@asu.edu

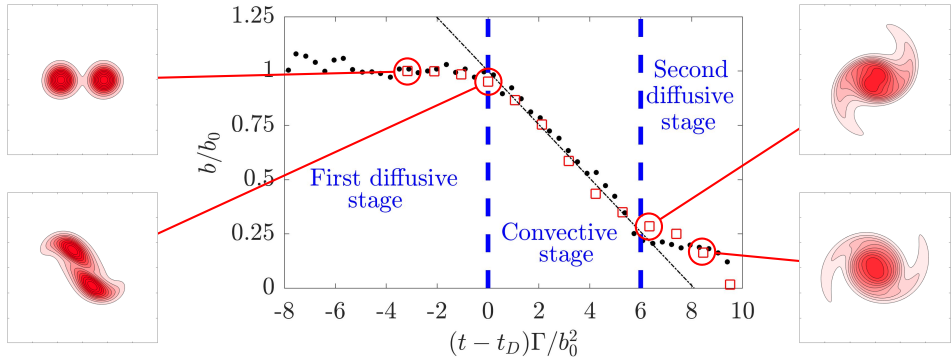


Figure 1: The evolution of vortex separation  $b/b_0$  as a function of time in single-phase fluid at  $Re_\Gamma = 530$ . Symbols:  $\bullet$ , Cerretelli & Williamson (2003);  $\square$ , present simulation. Snapshots represent normalized vorticity.

when  $a/b \sim (a/b)_{\text{crit}}$ . During this stage, the induced velocity pulls the two vortices together resulting in the two vortices becoming intertwined. Viscous diffusion activates once more to smooth the large vorticity gradients resulting from the merger. A single elliptical vortex remains at the end.

To the best of our knowledge, vortex merger in dusty flows has not been previously investigated. Yet, the dynamics in these flows may deviate considerably from those in particle-free flows. This is especially true for dusty flows with particle volume fraction greater than  $\phi > 10^{-5}$ , since this leads to a significant feedback force from the particles on the fluid. In this so-called two-way coupling regime, the dispersed phase may cause large flow modulation Kasbaoui *et al.* (2019). Recently, we have shown that the interaction between dispersed inertial particles and a single vortex alters the dynamics from what is commonly understood from particle-free vortex dynamics (Shuai & Kasbaoui 2022; Shuai *et al.* 2022). For example, a two-way coupled dusty Lamb-Oseen vortex decays significantly faster than a particle-free one (Shuai & Kasbaoui 2022). This enhanced decay is due to the ejection of inertial particles from the vortical core. While the particles cluster into a ring surrounding the vortex, their feedback force on the fluid leads to faster decay of the flow structure. Perhaps an even more striking effect is the fact that two-way coupled inertial particles dispersed in the core of a two-dimensional vortex trigger an instability (Shuai & Kasbaoui 2022). This is in contrast to the remarkable stability of particle-free vortices to two-dimensional perturbations (Fung & Kurzweg 1975). We have shown in (Shuai & Kasbaoui 2022) that the ejection of the particles from the vortex core activates a centrifugal Rayleigh-Taylor instability, that persists even for non-inertial particles.

In light of these previous findings, it is expected that the merger dynamics in two-way coupled dusty flows will be considerably different from those noted by Cerretelli & Williamson (2003). In the present study, we revisit the problem of co-rotating vortices with equal strength, augmented with mono-disperse inertial particles. We use Eulerian-Lagrangian simulations to show new merger mechanisms that depend on the particle inertia. A surprising outcome is that inertial particles may even temporarily push apart the two vortices.

## 2. Particle-free vortex merger

Before addressing how inertial particles may modulate the merger dynamics, we first describe the different stages of vortex pair merger in a particle-free case that will be used in §3 to

assess the effect of introducing inertial particles. The particle-free case considered matches the experiments of Cerretelli & Williamson (2003), and is characterized by a circulation Reynolds number  $Re_\Gamma = \rho_f \Gamma / \mu_f = 530$ , where  $\Gamma$  is the vortex circulation,  $\rho_f$ , and  $\mu_f$  are the fluid density and viscosity, respectively. In the following simulations, two co-rotating Lamb-Oseen vortices with equal radii  $a$  are initialized with a separation  $b_0$ , such that the ratio  $a/b_0 = 0.17$  is initially below the merger threshold  $(a/b)_{\text{crit}} = 0.29$ . This indicates that the two vortices will not merge immediately, but rather undergo a first diffusive stage before the onset of a convective stage. The angular velocity is defined as  $\omega_\Gamma = \Gamma / (2\pi a^2)$ . The Navier-Stokes equations are integrated using the computational approach described in (Shuai *et al.* 2022; Shuai & Kasbaoui 2022). The simulation grid is uniform with a high spatial resolution  $a/\Delta x \approx 51$  to provide good resolution of the vortex cores.

According to Cerretelli & Williamson (2003), the merger of two co-rotating vortices follows three stages called the first diffusive stage, the convective stage, and the second diffusive stage. All these stages are reproduced in our simulations as can be seen in figure 1 which show the evolution of the normalized vortex separation  $b/b_0$ , and normalized axial vorticity, respectively. The two vortices rotate around one another, but their separation remains constant as can be seen in figure 1. After a time period  $t_D$ , the cores grew sufficiently to reach the merger threshold  $(a/b)_{\text{crit}} = 0.29$ , and the convective merger is initiated. During this stage, the separation decreases linearly. The vortices are deformed significantly as shown at  $(t - t_D)\Gamma/b_0^2 = 0$  and 6 in figure 1. The second diffusive stage occurs between  $6 \lesssim (t - t_D)\Gamma/b_0^2 \lesssim 9$ , after which the vortex pair can be considered fully merged.

### 3. Particle-laden vortex merger

#### 3.1. Simulation configuration and vortex center identification

We now reconsider the merger of the vortex pair in §2 under dusty flow conditions, i.e., now, we consider the effects of dispersed particles on the merger dynamics. To that end, we conduct pseudo-2D Eulerian-Lagrangian simulations with the same methodology previously deployed in (Shuai & Kasbaoui 2022) and (Shuai *et al.* 2022). Except for the introduction of randomly placed particles, the simulation configuration remains the same as described in §2. The particles have diameter  $d_p$ , density  $\rho_p$ , and are initialized with velocities that match the fluid velocity at their locations.

We consider seven cases where the particle inertia and mass loading are varied. Table 1 lists a summary of the non-dimensional parameters in each case. Case A is the reference particle-free case. Cases B and C correspond to the limit of very low particle inertia, characterized by Stokes number  $St_\Gamma = \tau_p / \tau_f$ . Here  $\tau_p = \rho_p d_p^2 / 18\mu_f$  and  $\tau_f = 2\pi r_c^2 / \Gamma$  are particle response time and fluid response time in vortex flow. In these two cases,  $M = \langle \phi \rangle \rho_p / \rho_f = 0.5$  or 1.0 and is varied by varying the average particle volume fraction  $\langle \phi \rangle$ . In cases D-G, the Stokes number  $St$  is varied by changing the particle diameter as shown in Table 1. For all cases, the separation ratio is  $r_c/b_0 = 0.17$  and the density ratio  $\rho_p/\rho_f$  is fixed at 2167.

The instantaneous vortex separation, i.e., the distance between two vortex centers, is a significant variable to investigate the vortex merger process. Unlike in particle-free merger where smooth vorticity fields allow easy detection of the centers, the feedback force from dispersed particles causes large vorticity fluctuations that make the detection of vortex center harder. The left picture in figure 2 shows an example of the large vorticity fluctuations obtained in a particle-laden case. Due to this, we have found it necessary to filter the data from Euler-Lagrangian simulations to reliably detect the vortex centers.

To identify the vortex center, we first compute the filtered vorticity  $\bar{\omega}_z(\mathbf{x})$  from the original vorticity field  $\omega_z(\mathbf{y})$  by convolving with a triangle filter kernel  $g$  with support  $\delta_f$ . To retain

Case	St	$M$	$\langle \phi \rangle$	$r_c/d_p$
A	–	–	–	–
B	0.01	1	$4.6 \times 10^{-4}$	1008
C	0.01	0.5	$2.3 \times 10^{-4}$	1008
D	0.05	1	$4.6 \times 10^{-4}$	450
E	0.1	1	$4.6 \times 10^{-4}$	318
F	0.2	1	$4.6 \times 10^{-4}$	225
G	0.3	1	$4.6 \times 10^{-4}$	184

Table 1: Non-dimensional parameters considered in simulations. For all cases, the initial separation ratio is  $a/b_0 = 0.17$  and Reynolds number  $Re_\Gamma = \Gamma/\nu = 530$ .

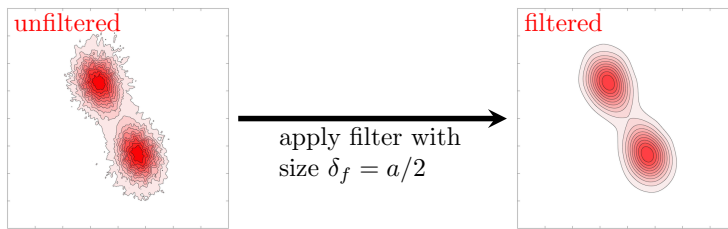


Figure 2: To detect vortex centers, the vorticity field is filtered to remove fluctuations induced by the Lagrangian forcing.

the vortex feature after the filtering process,  $\delta_f$  is set to be half of the initial vortex core radius, that is  $a_0/2$ . The right picture in figure 2 shows the result of applying this filtering procedure to the field in the left side of figure 2. The gradient descent method is then applied to locate the vortex centers.

### 3.2. Weakly inertial particles

Figure 3 shows the isocontours of normalized particle volume fraction and normalized filtered vorticity from  $t\Gamma/b_0^2 = 0$  to 14 for  $St = 0.01, 0.1$  and  $0.3$  with mass loading  $M = 1$ . Videos of these cases are provided in supplementary materials. From the snapshots in figure 3, it is clear that semi-dilute inertial particles alter the merger dynamics even at very small Stokes numbers. For the case at  $St = 0.01$ , shown on the first and second rows of figure 3, the dynamics of the vorticity field remain qualitatively similar to those of the particle-free vortex pair, however, the merger takes significantly longer and the vortices are further stretched than in the single-phase case. During this process, the particles are gradually ejected from the two vortex cores under the effect of preferential concentration (Shuai & Kasbaoui 2022). By  $t\Gamma/b_0^2 = 7$ , this results in the formation of two distinct void fraction bubbles. These structures get progressively larger and more stretched, as can be seen at  $t\Gamma/b_0^2 = 10.5$  and 14. As the vortices approach one another, a line of particles can be seen dividing the two vortices at  $t\Gamma/b_0^2 = 14$ . This line of particles forms because the region between the two vortices is dominated by straining, which draws in particles originally located outside the vortices, and those that have been ejected from the cores.

Figure 4a shows the evolution of the vortex-pair separation for the particle free case A, and cases B ( $St_\Gamma = 0.01, M = 1.0$ ) and C ( $St_\Gamma = 0.01, M = 0.5$ ). While the particle-free vortices merge around  $t\Gamma/b_0^2 \approx 16$ , merger occurs around  $t\Gamma/b_0^2 \approx 28$  with mass loadings  $M = 0.5$  and 1.

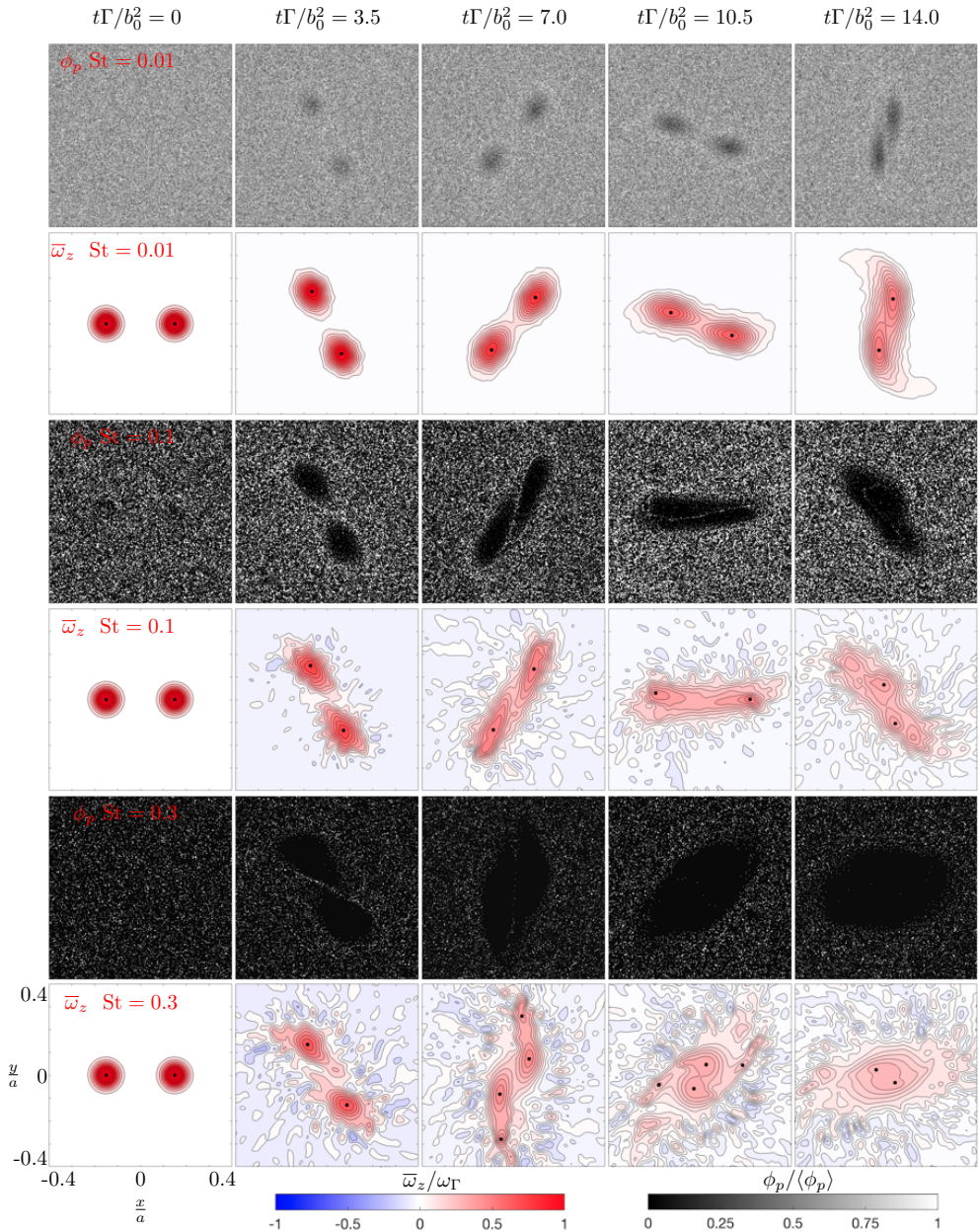


Figure 3: Successive snapshots of particle volume fraction  $\phi$  and filtered vorticity  $\bar{\omega}_z$  iso-contours for cases B, E, and G. See supplementary materials for animations.

The observation in figures 3 and 4a suggest that, at first approximation, the merger of dusty vortex pair at  $St \ll 1$  is similar to the merger of particle-free vortices in an effective fluid with density  $\rho_{\text{eff}} = (1 + M)\rho_f$ . To justify this reasoning, consider a Two-Fluid model of the particle phase where the particle velocity field is expanded in the limit of small inertia as

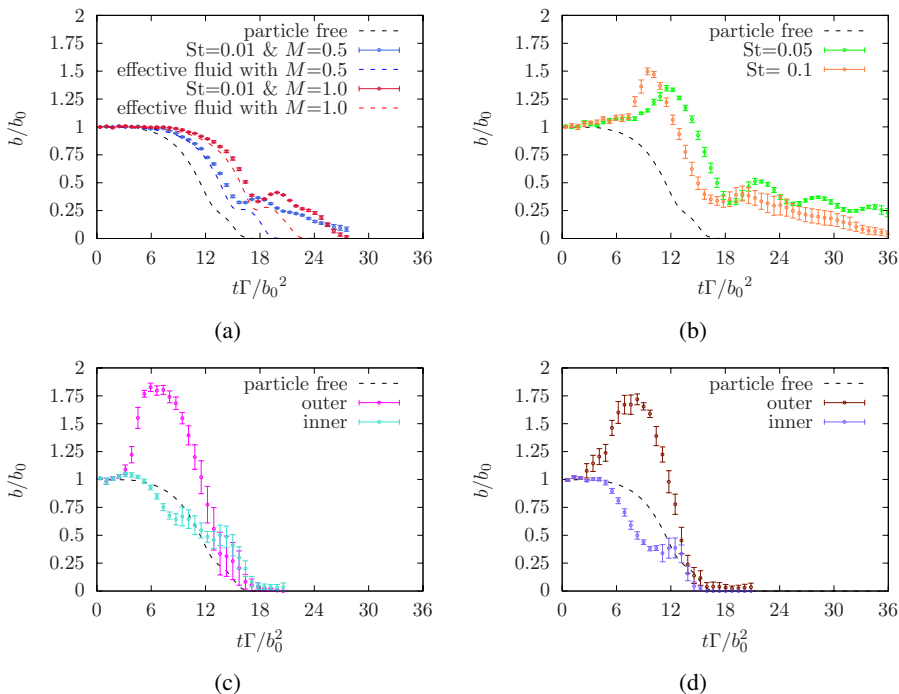


Figure 4: Evolution of the normalized separation  $b/b_0$  for (a) the weakly inertia cases B-C, (b) the moderately inertial cases D and E, and the highly inertial cases (c) F, and (d) G.

done in (Kasbaoui *et al.* 2015; Shuai *et al.* 2022)

$$\frac{\partial \phi}{\partial t} + \mathbf{u}_p \cdot \nabla \phi = -\phi \nabla \cdot \mathbf{u}_p, \quad (3.1)$$

$$\mathbf{u}_p = \mathbf{u}_f - \tau_p \left( \frac{\partial \mathbf{u}_f}{\partial t} + \mathbf{u}_f \cdot \nabla \mathbf{u}_f \right) + O(\tau_p^2), \quad (3.2)$$

Combining these equations with the fluid conservation equations

$$\nabla \cdot \mathbf{u}_f = 0, \quad (3.3)$$

$$\rho_f \left( \frac{\partial \mathbf{u}_f}{\partial t} + \mathbf{u}_f \cdot \nabla \mathbf{u}_f \right) = -\nabla p + \mu \nabla^2 \mathbf{u}_f + \frac{\rho_p \phi}{\tau_p} (\mathbf{u}_p - \mathbf{u}_f), \quad (3.4)$$

yields the following mixture equations

$$\frac{\partial \rho_{\text{eff}}}{\partial t} + \mathbf{u}_f \cdot \nabla \rho_{\text{eff}} = \tau_p \left\{ (\rho_{\text{eff}} - \rho_f) \nabla \mathbf{u}_f : \nabla \mathbf{u}_f + \frac{\nabla \rho_{\text{eff}}}{\rho_{\text{eff}}} \cdot (-\nabla p + \mu \nabla^2 \mathbf{u}_f) \right\}, \quad (3.5)$$

$$\rho_{\text{eff}} \left( \frac{\partial \mathbf{u}_f}{\partial t} + \mathbf{u}_f \cdot \nabla \mathbf{u}_f \right) = -\nabla p + \mu \nabla^2 \mathbf{u}_f, \quad (3.6)$$

where  $\rho_{\text{eff}} = \left( 1 + M \frac{\phi}{\langle \phi \rangle} \right) \rho_f$  is the local effective density, the first term on the right-hand side of (3.5) represents preferential concentration and the second term is due to the slip between the two phases. Thus, in the limit of negligible inertia, i.e.,  $\tau_p \rightarrow 0$ , or equivalently,  $\text{St}_\Gamma \rightarrow 0$ , the inertial effects due to preferential concentration and slip vanish making equations (3.5) and (3.6) identical to those of a single-phase fluid with effective density  $\rho_{\text{eff}}$ .

To verify this hypothesis, we conducted additional simulations of single-phase merger where the fluid density equals  $\rho_{\text{eff}} = (1 + M)\rho_f$  for  $M = 0.5$  and  $M = 1.0$ . Comparison of the vortex-pair separation from these simulations with the separation measured in the particle-laden cases B and C (see figure 4a) shows excellent agreement during most of the merger. Deviations that can be seen for  $t\Gamma/b_0^2 \gtrsim 18$  are likely due to inertial effects which, as suggested by the growth of the void bubbles, become significant as time progresses, despite the low Stokes number  $\text{St}_\Gamma = 0.01$ .

### 3.3. Moderately inertial particles

While the merger dynamics of a dusty flow with weakly inertial particles ( $\text{St}_\Gamma \ll 1$ ) are qualitatively similar to those of a particle-free flow, new dynamics emerge with increasing particle inertia. The most notable change noted in our simulations with  $0.05 \leq \text{St}_\Gamma \leq 0.2$  is that the eventual merger of the vortex pair starts first by the two vortices pushing apart.

The void bubbles in case E ( $\text{St}_\Gamma = 0.1$ ,  $M = 1.0$ ), shown in figure 3, grow significantly faster than in the low inertia case B, as the effects of preferential concentration intensify with increasing particle inertia (Shuai & Kasbaoui 2022). Further, the deformation of vortex cores and the void bubbles starts earlier suggesting that this process is related to the particle inertia. Due to the faster depletion of the cores, the particle line separating the two vortices appears earlier, at around  $t\Gamma/b_0^2 = 7$ , and becomes thinner as the merger progresses. During this early transient  $t\Gamma/b_0^2 \lesssim 10.5$ , the two cores push apart leading to an increase in the separation compared to the initial state. The cores start approaching one another only once the line of particles separating the cores becomes sufficiently thin, which eventually ruptures.

Figure 4b shows the evolution of the normalized separation  $b/b_0$  for cases D-E, alongside the data for the particle-free case A. While  $t\Gamma/b_0^2 \lesssim 5$ , the separation remains approximately constant. During this stage, the two vortices are mostly independent from one another and evolve according to dynamics similar to those reported in (Shuai & Kasbaoui 2022). Unlike in single-phase merger where the growth of the vortex cores is exclusively driven by viscosity, the growth of the cores and void bubbles are interlinked as the feedback force from the particles exiting the cores causes greater spreading of the vorticity field. Time  $t\Gamma/b_0^2 \simeq 5$  marks the start of a new stage, that we call repulsion stage, and which lasts until  $t\Gamma/b_0^2 \simeq 18$  at  $\text{St}_\Gamma = 0.05$  and  $t\Gamma/b_0^2 \simeq 16$  at  $\text{St}_\Gamma = 0.1$ . During this stage, the vortex pair separation increases reaching up to  $b/b_0 \sim 1.5$  at  $\text{St}_\Gamma = 0.1$ , which appears to be a saturation limit. At the end of this stage, the two void regions have merged, resulting in a large particle-free region containing the two vortices. The dynamics from here and onward follow those of single-phase merger.

To elucidate the mechanism driving the repulsion stage, we follow the approach of Cerretelli & Williamson (2003), in which vorticity field is decomposed into symmetric and antisymmetric components. We first rotate the filtered vorticity field  $\bar{\omega}_z(x, y)$  so that the two vortex centers lay on the horizontal line. Figure 5(a) shows the filtered vorticity field  $\bar{\omega}_z(x, y)$  without the rotation and figure 5(b) shows the vorticity field  $\bar{\omega}_z(x', y')$  after the rotation. The rotated vorticity  $\bar{\omega}_z(x', y')$  is then decomposed as

$$\bar{\omega}_z(x', y') = \frac{1}{2} [\bar{\omega}_z(x', y') + \bar{\omega}_z(-x', y')] + \frac{1}{2} [\bar{\omega}_z(x', y') - \bar{\omega}_z(-x', y')] = \bar{\omega}_S + \bar{\omega}_A \quad (3.7)$$

where  $\bar{\omega}_S$  is the symmetric vorticity and  $\bar{\omega}_A$  is the antisymmetric vorticity, as shown in figure 5(c) and figure 5(d) respectively. As argued by Cerretelli & Williamson (2003), it is only the antisymmetric vorticity field  $\bar{\omega}_A$  that contributes to the change of separation. Depending on the symmetries of  $\bar{\omega}_A$ , the induced velocity field may either pull together or push apart the vortex cores. Figure 6 shows the antisymmetric vorticity field for the cases of  $\text{St}_\Gamma = 0.01$ ,

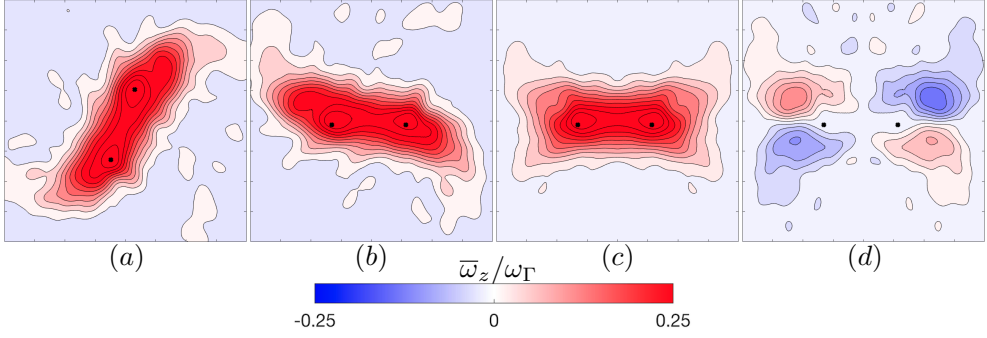


Figure 5: (a) Iso-contours of filtered vorticity  $\bar{\omega}_z(x, y)$ . (b) Iso-contours of rotated vorticity  $\bar{\omega}_z(x', y')$ . (c) Symmetric vorticity  $\bar{\omega}_S$ . (d) Antisymmetric vorticity  $\bar{\omega}_A$ .

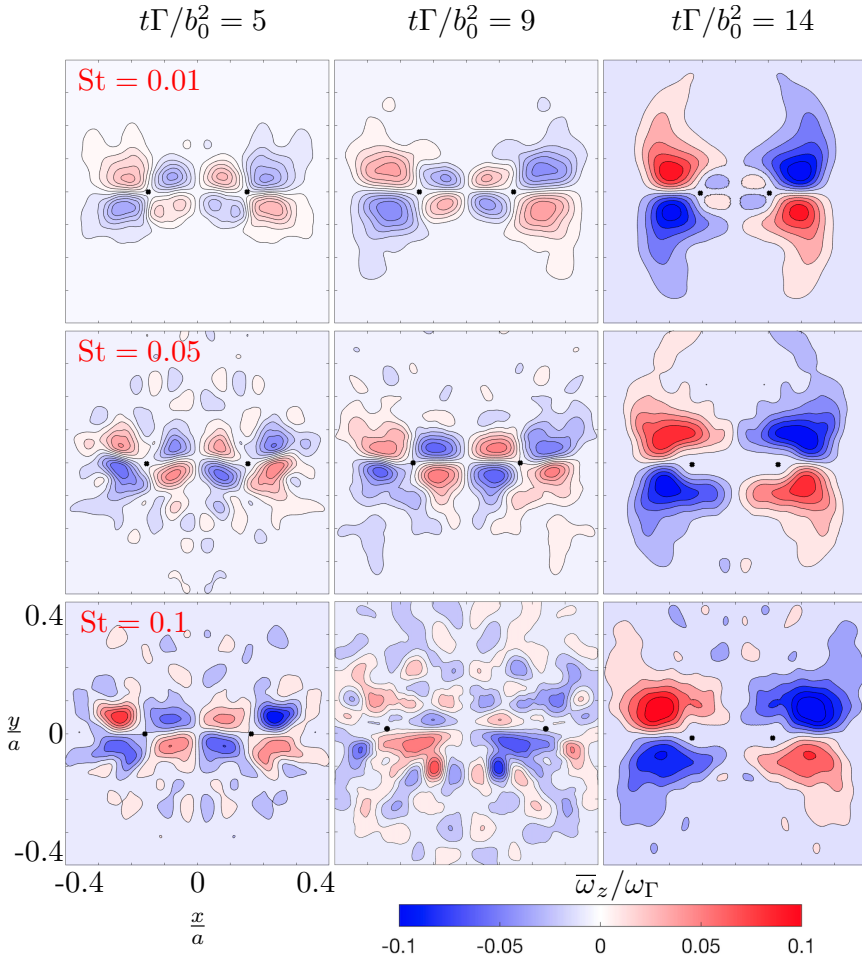


Figure 6: Iso-contours of antisymmetric vorticity  $\bar{\omega}_A$  for the case of  $St_\Gamma = 0.01, 0.05$  and  $0.1$  at non-dimensional times  $t\Gamma/b_0^2 = 5, 9$  and  $14$ ,  $Re_\Gamma = 530$ .

0.05 and 0.1 at successive instants. It is seen that for all cases the vorticity field has four pairs of counter-rotating vortices except for the later time around  $t\Gamma/b_0^2 = 14$ . The induced velocity from two inner vortex pairs pushes the two vortex centers apart, whereas the velocity generated from two outer counter-rotating vortex pairs pulls the two centers together. The vorticity intensity difference between inner side and outer side determines the change of separation. At  $t\Gamma/b_0^2 = 5$ , it is seen that the vorticity intensity of two inner vortex pairs is roughly equal to that of two outer pairs, resulting in the stable separation distance between two vortex centers at an early time when  $t\Gamma/b_0^2 \leq 5$  during the first diffusive stage. At  $t\Gamma/b_0^2 = 9$ , contrary to the low inertia case ( $St = 0.01$ ) where two inner vortex pairs are smaller than the outer pairs, the presence of moderate inertial particles ( $St = 0.05$  and  $0.1$ ) induces larger inner side vorticity, leading to the increase of separation when  $5 \leq t\Gamma/b_0^2 \leq 11$ , as shown in 4b. Whereas the separation decreases for  $St = 0.01$  during this period. At  $t\Gamma/b_0^2 = 14$ , figure 6 shows that the vorticity intensity of outer side is much larger than the inner side for all three cases, which causes a rapid merger of two co-rotating vortices at later time.

### 3.4. Highly inertial particles

With increasing Stokes number, the feedback force from the particles increasingly distorts the vortical structures making the merger murkier. This is illustrated in case G ( $St_\Gamma = 0.3$ ,  $M = 1$ ), in figure 3, where the vortices appear highly stretched at the early time  $t\Gamma/b_0^2 = 3.5$ . This extreme distortion causes each vortex to split into two smaller vortices, an inner one and an outer one, as can be clearly seen at  $t\Gamma/b_0^2 = 7$ . From figure 4c and 4d, the inner vortices start merging around  $t\Gamma/b_0^2 = 18$  for case F ( $St_\Gamma = 0.2$ ) and  $t\Gamma/b_0^2 = 14$  for case G ( $St_\Gamma = 0.3$ ), with no repulsion stage. Meanwhile, the outer vortices start with a repulsive stage for  $3 \lesssim t\Gamma/b_0^2 \lesssim 9$ , during which the centers push apart to a maximum distance  $b/b_0 \simeq 1.9$ . This stage is followed by a convective stage and a second diffusive stage between  $9 \lesssim t\Gamma/b_0^2 \simeq 16$ . At the end, a single distorted vortex is left, enclosed inside a larger void fraction bubble.

## 4. Conclusion

Eulerian-Lagrangian simulations of the merger of co-rotating vortices laden with inertial particles reveal new mechanics specific to dusty flows. The present simulations were carried out in the semi-dilute regime, specifically for particle volume fractions  $\langle\phi\rangle = 2.3 - 4.6 \times 10^{-4}$  and mass loading  $M = 0.5 - 1.0$ . Despite the low particle concentration, dusty flows in this regime have strong momentum coupling between the carrier and disperse phase since the mass loading is order unity. To investigate the effect of particle inertia, we varied the Stokes number  $St_\Gamma$  in the range 0.01 to 0.3. We found that these particles can be classified into three main categories. Particles that have a Stokes number  $St_\Gamma \leq 0.01$  are considered weakly inertial. With such particles, the merger of dusty vortices is delayed compared to the merger of particle-free vortices. However, the merger dynamics are not much different from those of the particle-free case, if one considers the particle-fluid mixture as an effective fluid with density  $\rho_{\text{eff}} = (1+M)\rho_f$ . Particles with Stokes number in the range  $\sim 0.05$  to  $\sim 0.2$  are considered as moderately inertial. In this case, the merger of a dusty vortex pair exhibits an additional stage characterized by a temporary repulsion of the vortex cores, before undergoing successive convective merger and second diffusive stages. Analyzing the antisymmetric vorticity field, we find that the vortex separation increase is caused by a repulsive force generated by the ejection of particles from the vortex cores. Once all particles have been ejected from the inner region separating the two cores, the merger is initiated and follows dynamics similar to those of particle-free vortex pairs. Highly inertial particles are those with  $St_\Gamma \gtrsim 0.3$ . The merger

becomes murkier, as the feedback force from these particles distorts significantly the vortex cores. For the case with  $St_{\Gamma} = 0.3$ , we find that each vortex splits into two parts and that the inner vortices merger first followed by the outer ones. In all cases, the final outcome of the merger is a single vortex with a core that is depleted from all particles and a surrounding halo of high particle concentration.

**Acknowledgments.** The authors acknowledge support from the US National Science Foundation (award #2148710, CBET-PMP), and from IIT Madras for the “Geophysical Flows Lab” research initiative under the Institute of Eminence framework.

**Declaration of Interests.** The authors report no conflict of interest.

#### REFERENCES

- CERRETELLI, C. & WILLIAMSON, C.H.K. 2003 The physical mechanism for vortex merging. *Journal of Fluid Mechanics* **475**, 41–77.
- FUNG, Y.T. & KURZWEIG, U.H. 1975 Stability of swirling flows with radius-dependent density. *Journal of Fluid Mechanics* **72(2)**, 243–255.
- GRIFFITHS, R.W. & HOPFINGER, E.J. 1987 Coalescing of geostrophic vortices. *Journal of Fluid Mechanics* **178**, 73–97.
- KASBAOUI, M.H., KOCH, D.L. & DESJARDINS, O. 2019 Clustering in Euler–Euler and Euler–Lagrange simulations of unbounded homogeneous particle-laden shear. *Journal of Fluid Mechanics* **859**, 174–203.
- KASBAOUI, M. H., KOCH, D. L., SUBRAMANIAN, G. & DESJARDINS, O. 2015 Preferential concentration driven instability of sheared gas–solid suspensions. *Journal of Fluid Mechanics* **770**, 85–123.
- MELANDER, M.V., ZABUSKY, N.J. & MCWILLIAMS, J.C. 1988 Symmetric vortex merger in two dimensions: Causes and conditions. *Journal of Fluid Mechanics* **195**, 303–340.
- OVERMAN, EDWARD A. & ZABUSKY, NORMAN J. 1982 Evolution and merger of isolated vortex structures. *The Physics of Fluids* **25** (8), 1297–1305.
- ROBERTS, K.V. & CHRISTIANSEN, J.P. 1972 Topics in computational fluid mechanics. *Computer Physics Communications* **3**, 14–32.
- ROSSOW, V.J. 1977 Convective Merging of Vortex Cores in LiftGenerated Wakes. *Journal of Aircraft* **14** (3), 283–290.
- SHUAI, S., DHAS, D.J., ROY, A. & KASBAOUI, M.H. 2022 Instability of a dusty vortex. *Journal of Fluid Mechanics* **948**, A56.
- SHUAI, S. & KASBAOUI, M.H. 2022 Accelerated decay of a Lamb-Oseen vortex tube laden with inertial particles in Eulerian-Lagrangian simulations. *Journal of Fluid Mechanics* **936**, A8.